Volume 52
Number 15
21 April 2023
Pages 4619-4986

Dalton Transactions

An international journal of inorganic chemistry

rsc.li/dalton

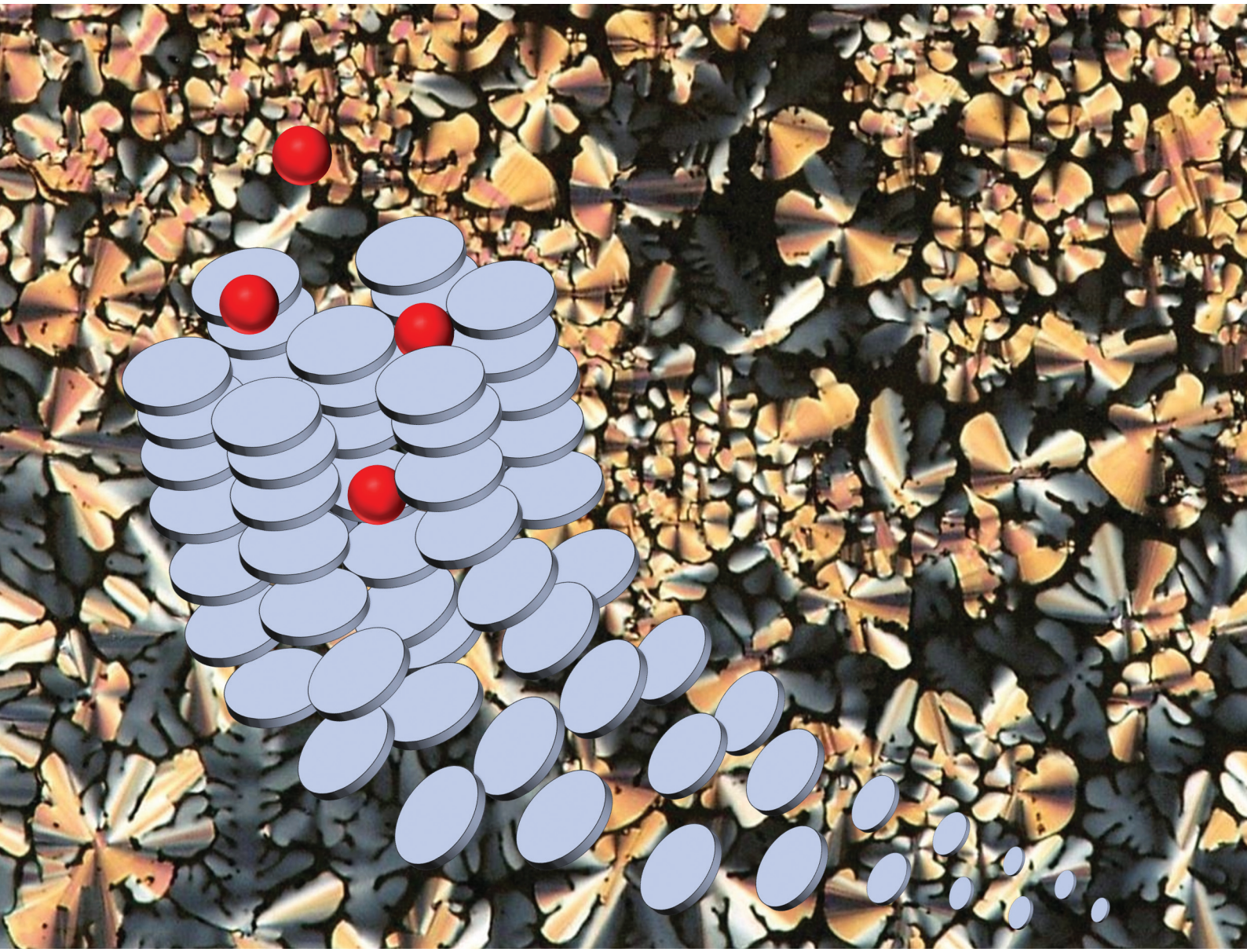

ISSN 1477-9226

ROYAL SOCIETY OF CHEMISTRY

PAPER

Cristián Cuerva, Rainer Schmidt *et al.*
Improving the mesomorphism in bispyrazolate Pd(II) metallomesogens: an efficient platform for ionic conduction

Dalton Transactions

ROYAL SOCIETY OF CHEMISTRY

PAPER

View Article Online
View Journal | View Issue

Check for updates

Cite this: *Dalton Trans.*, 2023, **52**, 4684

Improving the mesomorphism in bispyrazolate Pd(II) metallomesogens: an efficient platform for ionic conduction†

Cristián Cuerva, *[a] Mercedes Cano [a] and Rainer Schmidt *[b]

Received 21st November 2022,
Accepted 6th February 2023

DOI: 10.1039/d2dt03754h

rsc.li/dalton

The introduction of structural asymmetry in metallomesogens is an established strategy to improve their mesomorphic behaviour in terms of lower melting temperatures and higher stability ranges of the mesophase, which is particularly important for metallomesogens that have potential application as electrolytes that require wide operational temperature ranges. Here in this work, a novel series of unsymmetrical bis(isoquinolinylpyrazolate)palladium(II) compounds bearing four alkyl side-chains with different lengths are described. Rectangular and hexagonal columnar mesophases were formed with low melting temperatures of 42–45 °C in most cases, whereas the clearing temperatures reached values up to 412 °C. The charge transport properties have been studied by complex impedance spectroscopy, showing that the mesophase favours proton conduction in the absence of water or humidity. The exceptional thermal stability of these species makes them promising candidates to act as a platform for ionic conduction *via* the nanochannels originated in the columnar mesophases. The results presented confirm that introducing structural asymmetry in the Pd(II) metallomesogens studied is a valid strategy to enhance the liquid crystalline properties, which opens new ways to develop water-free electrolytes based on unsymmetrical bis(isoquinolinylpyrazolate) Pd(II) compounds for potential applications such as proton exchange membranes (PEMs).

Introduction

Pyrazolate ligands have been extensively studied in the last decades as building blocks for the design of metallomesogens with different liquid-crystalline phases and functionalities. In 1998, Kim *et al.* reported the first cyclic trinuclear Au(I) metallomesogen built with pyrazolate ligands that bear a unique alkyl chain of seven or eight carbon atoms. Both derivatives form hexagonal columnar mesophases with low stability ranges of 13 and 24 °C, respectively, *i.e.* the clearing temperatures are only 13 and 24 °C higher than the melting temperatures.[1] These compounds have only three side-chains, but they form Au dimers *via* stacking of two molecules mediated by intermolecular Au···Au interactions, leading to a disc-like structure with a total of six side-chains that induce the formation of the columnar mesophase. This strategy has been used frequently in various studies to prepare a great variety of cyclic trinuclear compounds with mesomorphic properties,[2–7] where the metal centre seems to play a key role with regard to the specific structures formed by self-assembly in the mesophase. Whereas alkyloxyphenyl pyrazolate-based Au(I) compounds form cyclic trimers, analogous Ag(I) compounds form open oligomers due to the labile nature of the Ag–N bond.[8]

Square-planar coordination environments can be achieved by using pyrazolate ligands in mono- and multinuclear non-cyclic species of Pd(II), Ni(II), Cu(II) and Pt(II).[9–11] This geometry generally facilitates the molecular self-assembly in the mesophase as a result of the establishment of metallophilic and/or π···π intermolecular interactions. On the other hand, the use of pyrazolates as a bridge ligand between two or more metal centres often leads to non-planar coordination environments. Although the geometry adopted in these species is usually not suitable to generate the supramolecular ordering required in the mesophase, Torralba *et al.* found that a series of dinuclear allyl–palladium compounds with two benzyl pyrazolate-binding ligands exhibit smectic A and smectic C mesophases.[12]

Besides, the distinct polarity in pyrazoles can favour both intramolecular and/or intermolecular interactions and therefore, induce the formation of highly stable mesophases. A clear example is the functionalisation of the pyrazole group with a pyridine moiety.[13] In this context, luminescent Ag(I) trimers have been described that can be transformed into 1D

[a]*MatMoPol Group. Department of Inorganic Chemistry, Faculty of Chemical Sciences, Complutense University of Madrid, Ciudad Universitaria, E-28040 Madrid, Spain. E-mail: c.cuerva@ucm.es*
[b]*GFMC. Departamento de Física de Materiales, Universidad Complutense de Madrid, Ciudad Universitaria, E-28040 Madrid, Spain. E-mail: rainer.schmidt@fis.ucm.es*

†Electronic supplementary information (ESI) available: ^{1}H and ^{13}C NMR spectra, DSC thermograms, and PXRD diffractograms. See DOI: https://doi.org/10.1039/d2dt03754h

oligomers.[3] Herein, the pyridyl nitrogen atom reinforces the cyclic self-assembly in the solid state *via* intramolecular interaction, but the labile nature of the Ag···N bond predominates by increasing the temperature and causes the opening of the cyclic system, leading to an oligomeric structure in the mesophase.

Furthermore, polycatenar pyridylpyrazole ligands have been used in deprotonated form to prepare bis(pyridylpyrazolate) Pt(II) compounds decorated with three long alkyl chains.[14] These compounds show both luminescence and hexagonal columnar mesophases in wide temperature ranges, and were used to fabricate the first prototype of polarised OLEDs based on metallomesogens.[15]

More recently, in 2017, a family of bis(isoquinolinylpyrazolate)-based Pd(II) compounds bearing four aliphatic chains have been studied. The isoquinoline group led to a stabilization of the columnar mesophases, increasing the clearing temperatures and achieving surprisingly wide stability ranges of the mesophase of 349 °C, *i.e.* the clearing temperature is 349 °C higher than the melting temperature in this case.[16] Both the fluid state of the mesophase and the nanochannels formed were found to enable reasonable proton conduction in the absence of water. Therefore, it was argued that these metallomesogens may have potential application as an electrolyte in PEM fuel cells.

Following up on this previous study,[16] the present work describes the synthesis of a new series of bis(isoquinolinylpyrazolate) Pd(II) metallomesogens [Pd($pz^{R(12,12)iq}$)($pz^{R(n,n)iq}$)] with four aliphatic chains of different length with n = 4–18, where the asymmetry is supposed to extend the existence ranges of the mesophases. It has been shown previously that the introduction of such asymmetry in metallomesogens is a viable strategy to improve the supramolecular ordering of the mesophase in terms of both a lower steric hindrance among the chains of neighbouring molecules and a reinforcement of the dipole–dipole interactions among them.[17–19] It is shown here that the compounds synthesized combine (i) the effect of the stabilisation of the mesophase due to the presence of the isoquinoline group and (ii) the effect of lowering the melting temperature due to the existence of molecular asymmetry.

Experimental section

Starting materials

Sodium hydride, Celite©, dichloromethane, chloroform and acetone were purchased from Sigma-Aldrich, Alfa Aesar and Scharlab, and were used without further purification. The starting pyrazoles and diiodide Pd(II) compounds were synthesized as reported previously.[20,21]

Synthesis and characterisation of compounds [Pd($pz^{R(12,12)iq}$)($pz^{R(n,n)iq}$)] 1–7

Two different solutions containing the corresponding diioide Pd(II) compound [$PdI_2(Hpz^{R(12,12)iq})$] (0.17 mmol) and the corresponding pyrazole ligand [$Hpz^{R(n,n)iq}$] (0.17 mmol) were prepared in 15 mL of CH_2Cl_2 each. Then, 60% NaH (0.34 mmol, 13.6 mg) was carefully added to both solutions, which were both stirred for 30 min at room temperature. Next, both solutions were mixed together and refluxed for 24 h. The resulting reaction mixture was concentrated until the formation of a yellow precipitate, which was then filtered and dissolved in 5 mL of chloroform. This new solution was then filtered over Celite© and concentrated until only 10 mL solution remained. Finally, the addition of 5 mL of acetone yields a pale-yellow solid that was filtered off and dried in vacuum.

[Pd($pz^{R(12,12)iq}$)($pz^{R(4,4)iq}$)] (1). Yellow solid (44%). Found: C, 69.8; H, 7.4; N, 7.2. $PdC_{68}H_{88}N_6O_4{\cdot}0.1CHCl_3$ requires C, 69.8; H, 7.6; N, 7.2%. ν_{max}/cm^{-1}: 2923–2853s ν(C–H)$_{aliph}$, 1638–1593s ν(C=C + C=N), 771–713m γ(C–H)$_{iq}$. δ_H (300.16 MHz; $CDCl_3$; TMS): 0.92 (6H, t, ^3J 6.8, CH_3), 1.10 (6H, t, ^3J 7.1, CH_3), 1.32 (40H, m, CH_2), 1.83 (8H, qt, ^3J 6.9, CH_2), 3.80 (4H, m, OCH_2), 3.82 (4H, m, OCH_2), 6.01 (2H, s, H4′), 6.24 (2H, br, Hp), 6.46 (4H, br, Ho), 6.86 (2H, s, H4), 7.12 (6H, m, H5, H7, H8), 7.40 (2H, br, H6), 10.23 (2H, s, H1).

[Pd($pz^{R(12,12)iq}$)($pz^{R(6,6)iq}$)] (2). Yellow solid (52%). Found: C, 71.1; H, 7.8; N, 6.9. $PdC_{72}H_{96}N_6O_4$ requires C, 71.1; H, 8.0; N, 6.9%. ν_{max}/cm^{-1}: 2923–2853s ν(C–H)$_{aliph}$, 1638–1594s ν(C=C + C=N), 775–713m γ(C–H)$_{iq}$. δ_H (300.16 MHz; $CDCl_3$; TMS): 0.91 (6H, t, ^3J 6.8, CH_3), 1.00 (6H, t, ^3J 6.7, CH_3), 1.31 (48H, m, CH_2), 1.85 (8H, qt, ^3J 6.9, CH_2), 3.86 (8H, t, ^3J 6.4, OCH_2), 6.16 (2H, s, H4′), 6.28 (2H, br, Hp), 6.59 (4H, br, Ho), 7.02 (2H, s, H4), 7.17 (2H, pt, ^3J 7.3, H7), 7.23 (2H, m, H5), 7.31 (2H, d, ^3J 7.6, H8), 7.47 (2H, pt, ^3J 7.6, H6), 10.40 (2H, s, H1).

[Pd($pz^{R(12,12)iq}$)($pz^{R(8,8)iq}$)] (3). Yellow solid (58%). Found: C, 71.4; H, 8.0; N, 6.8. $PdC_{76}H_{104}N_6O_4$ requires C, 71.8; H, 8.2; N, 6.6%. ν_{max}/cm^{-1}: 2923–2853s ν(C–H)$_{aliph}$, 1638–1593s ν(C=C + C=N), 775–713m γ(C–H)$_{iq}$. δ_H (300.16 MHz; $CDCl_3$; TMS): 0.91 (6H, t, ^3J 6.8, CH_3), 0.95 (6H, t, ^3J 6.5, CH_3), 1.31 (56H, m, CH_2), 1.85 (8H, qt, ^3J 6.8, CH_2), 3.86 (8H, t, ^3J 6.5, OCH_2), 6.16 (2H, s, H4′), 6.28 (2H, br, Hp), 6.59 (4H, br, Ho), 7.02 (2H, s, H4), 7.16 (2H, pt, ^3J 7.4, H7), 7.25 (2H, m, H5), 7.31 (2H, d, ^3J 7.7, H8), 7.48 (2H, pt, ^3J 7.4, H6), 10.39 (2H, s, H1). δ_C (75.48 MHz; $CDCl_3$; TMS): 14.2 (CH_3), 22.8–32.0 (CH_2), 67.5 (OCH_2), 98.0 (C4′), 99.2 (Cp), 101.7 (Co), 113.1 (C4), 125.1 (C10), 125.3 (C7), 125.8 (C5), 128.5 (C8), 130.9 (C6), 135.9 (C9), 136.7 (Ci), 145.3 (C3), 147.9 (C3′), 149.1 (C5′), 154.6 (C1), 159.5 (Cm).

[Pd($pz^{R(12,12)iq}$)($pz^{R(10,10)iq}$)] (4). Yellow solid (55%). Found: C, 72.1; H, 8.0; N, 6.4. $PdC_{80}H_{112}N_6O_4$ requires C, 72.3; H, 8.5; N, 6.3%. ν_{max}/cm^{-1}: 2922–2853s ν(C–H)$_{aliph}$, 1638–1594s ν(C=C + C=N), 775–713m γ(C–H)$_{iq}$. δ_H (300.16 MHz; $CDCl_3$; TMS): 0.91 (6H, t, ^3J 6.8, CH_3), 0.93 (6H, t, ^3J 6.6, CH_3), 1.34 (64H, m, CH_2), 1.84 (8H, qt, ^3J 6.9, CH_2), 3.86 (8H, t, ^3J 6.4, OCH_2), 6.12 (2H, s, H4′), 6.27 (2H, br, Hp), 6.56 (4H, br, Ho), 6.98 (2H, s, H4), 7.15 (2H, pt, ^3J 7.4, H7), 7.23 (2H, d, ^3J 8.2, H5), 7.28 (2H, m, H8), 7.46 (2H, pt, ^3J 7.3, H6), 10.36 (2H, s, H1).

[Pd($pz^{R(12,12)iq}$)($pz^{R(14,14)iq}$)] (5). Yellow solid (60%). Found: C, 73.9; H, 8.8; N, 5.4. $PdC_{88}H_{128}N_6O_4$ requires C, 73.4; H, 9.0; N, 5.8%. ν_{max}/cm^{-1}: 2919–2851s ν(C–H)$_{aliph}$, 1638–1593s ν(C=C + C=N), 776–713m γ(C–H)$_{iq}$. δ_H (300.16 MHz; $CDCl_3$;

TMS): 0.91 (12H, m, CH_3), 1.31 (80H, m, CH_2), 1.85 (8H, qt, ^3J 6.7, CH_2), 3.85 (8H, t, ^3J 6.4, OCH_2), 6.19 (2H, s, H4′), 6.29 (2H, br, Hp), 6.61 (4H, br, Ho), 7.05 (2H, s, H4), 7.18 (2H, pt, ^3J 7.5, H7), 7.26 (2H, m, H5), 7.34 (2H, d, ^3J 7.9, H8), 7.49 (2H, pt, ^3J 7.6, H6), 10.42 (2H, s, H1).

[Pd(pz$^{R(12,12)iq}$)(pz$^{R(16,16)iq}$] (6). Yellow solid (53%). Found: C, 74.1; H, 8.9; N, 5.4. $PdC_{92}H_{136}N_6O_4$ requires C, 73.8; H, 9.2; N, 5.6%. ν_{max}/cm^{-1}: 2918–2850s ν(C–H)$_{aliph}$, 1638–1593s ν(C═C + C═N), 776–712m γ(C–H)$_{iq}$. δ_H (300.16 MHz; $CDCl_3$; TMS): 0.89 (6H, t, ^3J 6.5, CH_3), 0.91 (6H, t, ^3J 6.5, CH_3), 1.31 (88H, m, CH_2), 1.84 (8H, qt, ^3J 6.8, CH_2), 3.84 (8H, t, ^3J 6.6, OCH_2), 6.11 (2H, s, H4′), 6.27 (2H, br, Hp), 6.55 (4H, br, Ho), 6.98 (2H, s, H4), 7.14 (2H, pt, ^3J 7.4, H7), 7.23 (2H, d, ^3J 8.2, H5), 7.26 (2H, m, H8), 7.46 (2H, pt, ^3J 7.3, H6), 10.34 (2H, s, H1).

[Pd(pz$^{R(12,12)iq}$)(pz$^{R(18,18)iq}$)] (7). Yellow solid (47%). Found: C, 74.3; H, 8.8; N, 5.2. $PdC_{96}H_{144}N_6O_4$ requires C, 74.3; H, 9.3; N, 5.4%. ν_{max}/cm^{-1}: 2914–2851s ν(C–H)$_{aliph}$, 1638–1593s ν(C═C + C═N), 771–713m γ(C–H)$_{iq}$. δ_H (300.16 MHz; $CDCl_3$; TMS): 0.88 (6H, t, ^3J 7.0, CH_3), 0.91 (6H, t, ^3J 6.5, CH_3), 1.30 (96H, m, CH_2), 1.84 (8H, qt, ^3J 6.7, CH_2), 3.84 (8H, t, ^3J 6.5, OCH_2), 6.12 (2H, s, H4′), 6.27 (2H, br, Hp), 6.56 (4H, br, Ho), 6.99 (2H, s, H4), 7.15 (2H, pt, ^3J 7.0, H7), 7.26 (4H, m, H5, H8), 7.46 (2H, pt, ^3J 7.3, H6), 10.36 (2H, s, H1).

Physical property measurements

Structural characterisation. The elemental analyses of C, H and N were performed by the Microanalytical Service at the Complutense University of Madrid using the elemental microanalyzer LECO CHNS932 3288 (validated range: %C 0.5–94.7, % H 0.5–7.6, %N 0.5–23.0). The infra-red spectra were recorded on a PerkinElmer Spectrum 100 FTIR spectrophotometer with a universal ATR accessory in the region of 4000–650 cm^{-1}: w (weak), m (medium) and s (strong). ^1H and ^{13}C NMR, 2D COSY, selective 1D NOESY, ^1H–^{13}C HMQC, and ^1H–^{13}C HMBC spectra were carried out on a Bruker DPX-300 spectrophotometer from the NMR Service at the Complutense University of Madrid. All measurements were performed with the samples dissolved in $CDCl_3$ solutions at room temperature. Chemical shifts δ are listed relative to $SiMe_4$ by using the signal of the deuterated solvent as a reference (7.26 and 77.0 ppm for ^1H and ^{13}C, respectively) and coupling constants J are given in hertz. Multiplicities are indicated as follows: s (singlet), d (doublet), t (triplet), pt (pseudo-triplet), qt (quintet), ddd (doublet of doublets of doublets), m (multiplet). The ^1H and ^{13}C chemical shifts are accurate to ±0.01 and ±0.1 ppm, respectively, and coupling constants to ±0.3 Hz.

Mesomorphism. Polarised optical microscopy (POM) observations were carried out by using an Olympus BX50 microscope equipped with a Linkam THMS 600 heating stage. The transition temperatures and their associated enthalpy data were determined with a PerkinElmer Pyris 1 differential scanning calorimeter. Samples were hermetically sealed in aluminium pans and measurements were carried out with heating and cooling rates of 10 K min^{-1}. Temperature-dependent powder X-ray diffraction (XRD) studies were carried out on a Panalytical X'Pert PRO MPD diffractometer with Cu-Kα (1.54 Å) radiation in a θ–θ configuration equipped with an Anton Paar HTK1200 heating stage (X-Ray Diffraction Service at the Complutense University of Madrid).

Charge transport and dielectric measurements

The charge transport and dielectric properties of the compounds in the solid and liquid crystal phases were studied by alternating current (AC) impedance spectroscopy using an Alpha Analyser integrated into the Novocontrol BDS 80. Measurements were performed at a frequency (f) range of 1 Hz–10 MHz with 6 measurements points per frequency decade, using a 0.1 V amplitude for the applied AC voltage signal. The temperature (T) was varied between 160 K and the upper instrumental limit of 562 K (−113 °C–289 °C) upon heating and cooling cycles. Impedance data were taken under steady state conditions, *i.e.* the temperature was stabilised for 3–10 minutes before taking impedance measurements over the full f-range. The temperature increments/reductions for taking impedance measurements were 20 K–2 K steps. In particular, the temperature was increased/decreased in smaller steps near the phase transitions. The compounds in the solid state were placed between the polished electrodes of a custom-built stainless-steel liquid cell with a high surface to thickness ratio. The cell was closed with a sapphire plate and placed inside the Novocontrol system.

The impedance response of the materials was obtained at the selected temperatures for heating and cooling cycles in terms of the real and imaginary parts (Z', Z'') of the complex impedance $Z^* = Z' + iZ''$. The data were converted into the complex conductivity σ^* and capacitance C^* notations, $\sigma^* = \sigma' + i\sigma''$ and $C^* = C' - iC''$, using the standard conversions: $Z^* = (g\sigma^*)^{-1}$, and $Z^* = (i\omega C^*)^{-1}$, where g (in cm) is the geometrical factor given by electrode area divided by electrode distance, and ω is the angular frequency. The geometrical factor g could only be estimated from the weight and density of the powder measured initially, and the measurement cell dimensions. Equivalent circuit fitting of the impedance data was performed by using commercial Z-View® software.

Results and discussion

Synthesis and structural characterisation

Novel unsymmetrical isoquinoline-functionalised Pd(II) compounds [Pd(pz$^{R(12,12)iq}$)(pz$^{R(n,n)iq}$)] **1–7** were synthesised from the related diiodide palladium derivatives and the corresponding pyrazoles, as described previously.[20,21] The reaction was carried out in two steps, the first one under basic conditions to deprotonate the pyrazole core of the diiodide derivatives, and the second one consisting in the addition of the corresponding pyrazole compound in a 1 : 1 ligand-to-complex molar ratio to be coordinated to the palladium centre (Scheme 1).

The full family of Pd(II) compounds was characterised comprehensively by IR, ^1H and ^{13}C NMR spectroscopy, and by elemental analyses. 2D COSY and selective 1D NOESY NMR

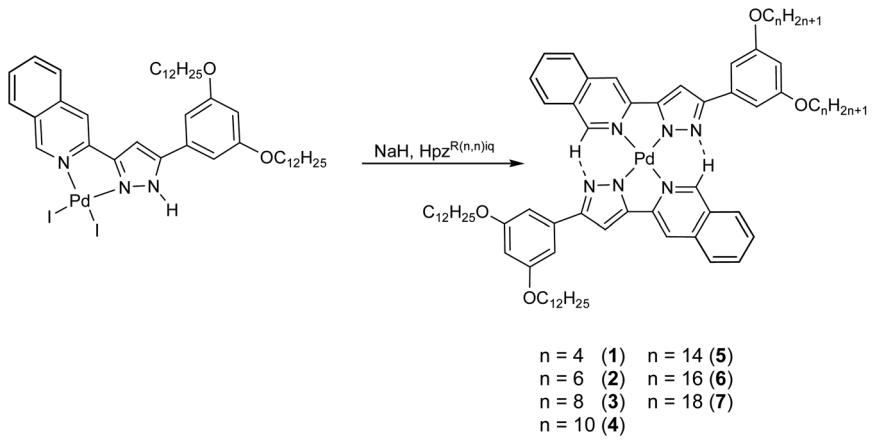

Scheme 1 Synthesis of unsymmetrical Pd(II) metallomesogens [Pd($pz^{R(12,12)iq}$)($pz^{R(n,n)iq}$)] **1–7**.

allowed for the unequivocal assignment of all proton resonances. A unique set of signals is observed for each aromatic proton, in agreement with the equivalence of the two aromatic systems in terms of the two bidentate coordinated ligands (Fig. S1a†). On the other hand, the proton signals associated with the –OCH_2– and –CH_3 groups at the alkyl chains appear duplicated. This effect is more noticeable in compounds with higher degree of asymmetry (Fig. S1b†), which clearly evidences the coordination of two ligands with different chain length. Likewise, DEPT (Distortionless Enhancement by Polarization Transfer) and 2D ^1H–^{13}C HMQC and HMBC NMR experiments were carried out for the correct interpretation of the ^{13}C NMR spectra (Fig. S2†). All the spectroscopic data are given in more detail in the ESI.†

Liquid crystal behaviour of compounds [Pd($pz^{R(12,12)iq}$)($pz^{R(n,n)iq}$)] 1–7

The study of the liquid crystal behaviour was carried out by polarised light optical microscopy (POM), differential scanning calorimetry (DSC) and powder X-ray diffraction (XRD). The results revealed that all compounds exhibit mesomorphism in wide temperature ranges, indicating that the asymmetrical character of these derivatives stabilizes the mesophases as desired. All melting and clearing temperatures established by POM and DSC, as well as the associated enthalpy data, are presented in Table 1 upon heating to the clearing point, followed by cooling. The DSC traces are given in Fig. S3–S9.†

The POM micrographs shown in Fig. 1 illustrate that the mesophases show the classic textures of columnar assemblies. Dendritic and pseudo-focal conic structures can be seen, emerging from the isotropic liquid upon cooling (Fig. 1a–c). The typical birefringent behaviour of these materials is also visible upon heating, when molecules present a high degree of long-range disorder in the mesophase (Fig. 1d).

The phase behaviour of these compounds strongly depends on the alkyl chain length. The DSC trace of the compounds with long alkyl chains (**5–7**) displays an endothermic peak at *ca.* 45 °C, which agrees with the formation of the columnar

Table 1 Phase transitions in the Pd(II) metallomesogens [Pd($pz^{R(12,12)iq}$)($pz^{R(n,n)iq}$)] **1–7**

	12/*n*	Transitions[a]	T^b [°C] (ΔH [kJ mol^{-1}])
1	12/4	Cr → Col_r → Col_h → I	59 (8.4), 92 (0.5), 369
		I → Col_h → Cr	355, 58
2	12/6	Cr → Col_r → Col_h → I	56 (1.7), 77 (23.3), 397
		I → Col_h → Cr	381, 25[c]
3	12/8	Cr → Col_r → Col_h → I	61 (31.3), 84 (10.9), 412
		I → Col_h → Cr	360, 25[c]
4	12/10	Cr → Col_r → Col_h → I	42 (5.2), 84 (22.3), 390
		I → Col_h → Cr	381, 25[c]
5	12/14	Cr → Col_h → I	45 (26.8), 371
		I → Col_h → Cr	358, 25[c]
6	12/16	Cr → Col_h → I	45 (17.9), 357
		I → Col_h → Cr	345, 25[c]
7	12/18	Cr → Col_h → I	42 (22.8), 330
		I → Col_h → Cr	300, 25[c]

[a] Cr = crystalline phase, Col_r = rectangular columnar mesophase, Col_h = hexagonal columnar mesophase, I = isotropic liquid. [b] DSC onset peaks. Enthalpies of the Col_h → I, I → Col_h and Col_h → Cr phase transitions were not determined due to partial decomposition; the corresponding temperatures are given by POM. [c] The liquid crystal phase remains metastable for several hours.

mesophase observed by POM (Fig. S7–S9†). XRD experiments confirm the hexagonal columnar nature of the mesophase (Table 2). However, two endothermic peaks are recorded in the DSC thermograms of compounds **1–4** at low temperatures (Fig. S3–S6†). The first one is attributed to the formation of a mesophase by optical observations, and the second one seems to suggest the formation of a second mesophase, since no changes were observed in their POM textures. In particular, for compound **2**, two overlapping exothermic peaks appear during the formation of the second mesophase (Fig. S4†). This may be due to a structural reorganization that occurs during the formation of this second mesophase, possibly consisting in the formation of metal–metal interactions, giving rise to a highly-ordered mesophase. The existence of two columnar mesophases in compounds **1–4** was confirmed by temperature-dependent XRD studies. Fig. 2 shows the diffractograms recorded for compound **4** at 60 °C and 100 °C. At 60 °C

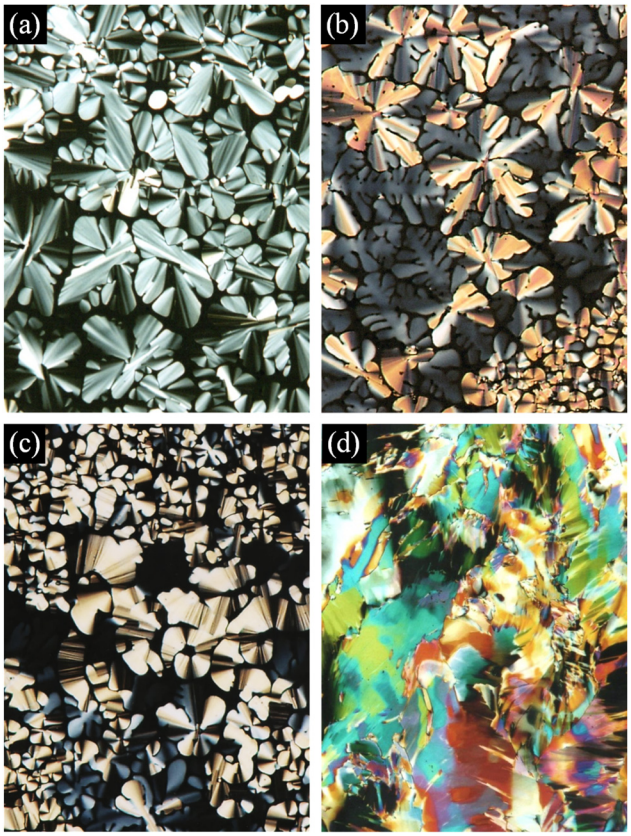

Fig. 1 POM images of the mesophase textures for compounds (a) [Pd(pz$^{R(12,12)iq}$)(pz$^{R(14,14)iq}$)] **5** at 190 °C on cooling, (b) [Pd(pz$^{R(12,12)iq}$)(pz$^{R(16,16)iq}$)] **6** at 139 °C on cooling, (c) [Pd(pz$^{R(12,12)iq}$)(pz$^{R(16,16)iq}$)] **6** at 139 °C on cooling, and (d) [Pd(pz$^{R(12,12)iq}$)(pz$^{R(18,18)iq}$)] **7** at 296 °C on heating.

Table 2 XRD data for the unsymmetrical Pd(II) compounds **4**, **5** and **6**

	Phase	*d*-Spacing (Å)	[*hkl*][a]	Parameters[c]
4	Col$_r$	25.9, 22.5, 18.3, 14.0, 13.0, 11.4, 8.7, 7.1, 6.5, 4.4, 3.4	110, 200, 210, 310, 220, 400, 330, 600, 620, alkyl[b], 001	a = 45.0 Å, b = 31.7 Å, V_{mol} = 2594 Å^3, S_{col} = 713 Å^2, h = 3.6 Å, T = 60 °C
	Col$_h$	22.7, 13.2, 11.4, 8.6, 4.9, 3.4	100, 110, 200, 210, alkyl[b], 001	a = 26.3 Å, V_{mol} = 2205 Å^3, S_{col} = 599 Å^2, h = 3.7 Å, T = 100 °C
5	Col$_h$	24.1, 14.1, 12.2, 5.2, 3.4	100, 110, 200, alkyl[b], 001	a = 28.1 Å, V_{mol} = 2594 Å^3, S_{col} = 684 Å^2, h = 3.8 Å, T = 150 °C
6	Col$_h$	24.2, 14.3, 12.4, 9.4, 4.6, 3.4	100, 110, 200, 210, alkyl[b], 001	a = 28.5 Å, V_{mol} = 2485 Å^3, S_{col} = 703 Å^2, h = 3.5 Å, T = 80 °C

[a] [*hkl*] are the Miller indices of the respective reflections. [b] Broad halo associated with the liquid-like order of the molten alkyl chains. [c] Molecular volume: $V_{mol} = M_w/(N_A{\cdot}\rho)$; where M_w is the molecular weight, N_A is Avogadro's number and ρ is the density (0.8–1.2 g cm^{-3}). For hexagonal columnar mesophases: lattice constant $a = 2[\sum d_{hk}\sqrt{(h^2 + k^2 + hk)}]/\sqrt{3}N_{hk}$, where N_{hk} is the number of $hk0$ reflections; columnar cross-section area $S_{col} = (\sqrt{3})a^2/2$. For rectangular columnar mesophases, lattice constants a and b were obtained as follows: $1/d_{hk}{}^2 = h^2/a^2 + k^2/b^2$, assigning the first peak to the (110) reflection and the second one to the (200) reflection; columnar cross-section area $S_{col} = a \times b/2$. Intracolumnar distance $h = V_{mol}/S_{col}$.

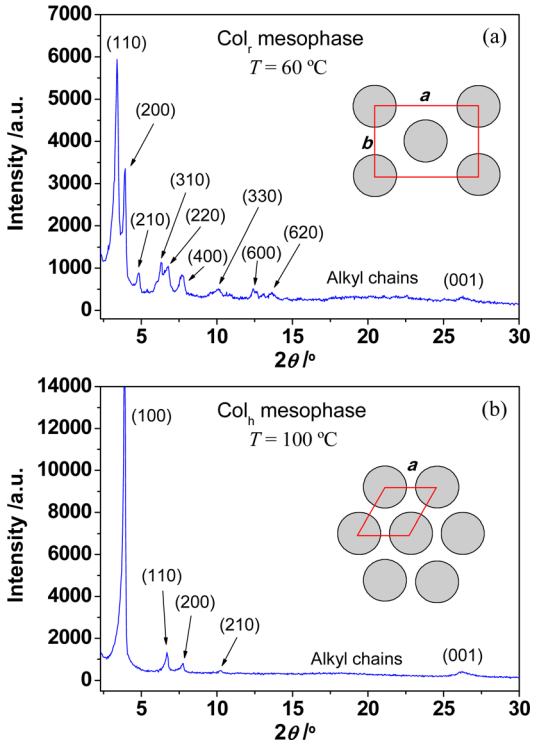

Fig. 2 XRD diffractograms for compound [Pd(pz$^{R(12,12)iq}$)(pz$^{R(10,10)iq}$)] **4** recorded at (a) 60 °C and (b) 100 °C, upon heating.

(Fig. 2a), the signal pattern is composed by a series of nine peaks that can be indexed to the (110), (200), (210), (310), (220), (400), (330), (600), (620) reflections of a rectangular lattice (a = 45.0 Å, b = 31.7 Å), associated with the rectangular columnar mesophase. By increasing the temperature, the XRD pattern drastically changes, now showing at 100 °C (Fig. 2b) a series of four reflections with the typical *d*-spacing ratio of a hexagonal columnar mesophase, $1:1/\sqrt{3}:1/\sqrt{4}:1/\sqrt{7}$. This fact clearly evidences the transformation of the Col$_r$ mesophase into a more stable Col$_h$ one, in agreement with the DSC studies.[22] The signal from the (100) reflection usually appears stronger and sharper than other signals reflecting long range orientational order of columnar mesophases. For both mesophases, the characteristic broad halo associated with the liquid-like order of the molten alkyl chains, and the stacking distance of the columnar mesophase were determined to be 4.4 Å and 3.4 Å, respectively.

In summary, compounds with longer alkyl chains ($n \geq 14$) form a Col$_h$ mesophase at temperatures of around 43 °C, whereas this mesophase appears at *ca.* 80–90 °C in compounds with short chains. This fact suggests an increasing of the stability of the Col$_h$ mesophase when long alkyl chains are used. The XRD patterns in the Col$_h$ mesophase for compounds **5** and **6** are shown in Fig. S10 and S11.† Note that weak and broad signals appear in the XRD diffractogram of **6**, which is a clear indication that this Col$_h$ mesophase presents a high degree of disorder. This feature is consistent with the increase of the alkyl chain length in **6** respect to compounds **4** and **5**.

Fig. 3 displays the stability ranges of the columnar mesophases for all Pd(II) metallomesogens. As expected, the presence of the isoquinoline group causes a remarkable increase of the clearing temperatures in comparison with related pyridylpyrazolate Pd(II) derivatives,[23] achieving surprisingly high values of up to 412 °C. This feature had previously been described for analogous symmetrical pyrazolate Pd(II) compounds.[16] It is noteworthy that the introduction of asymmetry in the pyrazolate ligands significantly reduces the melting point to near room temperature, improving the temperature range of the liquid crystal state for these asymmetric Pd(II) systems with respect to the symmetrical ones. This implies that the temperature range for potential applications of these novel compounds broadens. Since the columnar mesophases present nanochannels that can be used for the transport of charged particles, the characteristic proton conduction of these metallomesogens has been investigated.

Proton conduction in the liquid crystal state

The proton conductivity of the Pd(II) compounds [Pd(pz$^{R(12,12)iq}$)(pz$^{R(n,n)iq}$)] **2**, **4**, **5** and **7**, was determined in the solid state and in the mesophase using impedance spectroscopy. These compounds were selected as representative examples to evaluate the influence of the alkyl chain length on the charge transport and dielectric properties of these materials. The charge transport by proton conduction in this kind of bispyrazolate species has been related to a C–H···N proton transfer. Although it is not energetically favourable, the proton transfer occurs as a result of the fluidic nature of the mesophase and the existence of axial fluctuations, which boost the proton jump between neighbouring molecules.[24]

Fig. 4a shows the complex impedance plane plot of imaginary *vs.* real part of the impedance (–*Z*″ *vs.* *Z*′) in the Col$_h$ mesophase of sample **4**. The single slightly unsymmetrical semicircle that appears at high and intermediate frequencies represents the intrinsic dielectric contribution of the sample, and it can be well modelled by using two R–CPE elements in series, consisting of a resistor (R) and a constant phase element (CPE) that represents a non-ideal capacitor. This circuit model was also employed to fit the experimental data found in analogous symmetrical Pd(II) compounds, although the latter ones required the use of an additional ideal capacitor in one of the R–CPE elements to achieve a good fit of the impedance data at high frequencies.[16] The presence of an additional low-frequency contribution in form of a pike-like shape suggests charge blocking at the sample–electrode interface, which is consistent with a proton conduction mechanism. Keep in mind that proton charge carriers that are mobile within the molecular sample cannot easily cross the interface into the metallic electrodes, generating an interface dielectric contribution of large resistivity.[25] This can be confirmed from the dielectric permittivity *vs.* frequency curve from sample **4** plotted in Fig. 4b. The permittivity value abruptly increases at low frequency as a result of the highly resistive electrode/sample interface, where the high resistivity is associated with charge blocking at this interface.

The temperature-dependent conductivity curves for the main intrinsic dielectric contribution were obtained from the

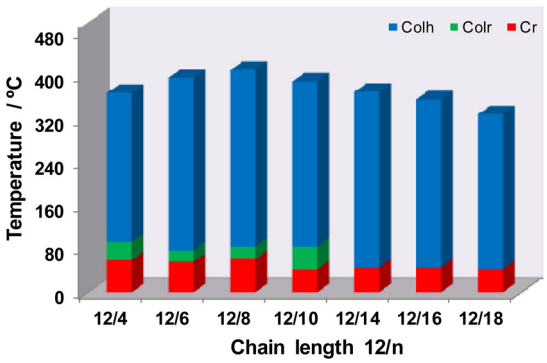

Fig. 3 Stability range of the columnar mesophases for the unsymmetrical Pd(II) metallomesogens [Pd(pz$^{R(12,12)iq}$)(pz$^{R(m,m)iq}$)] **1–7**.

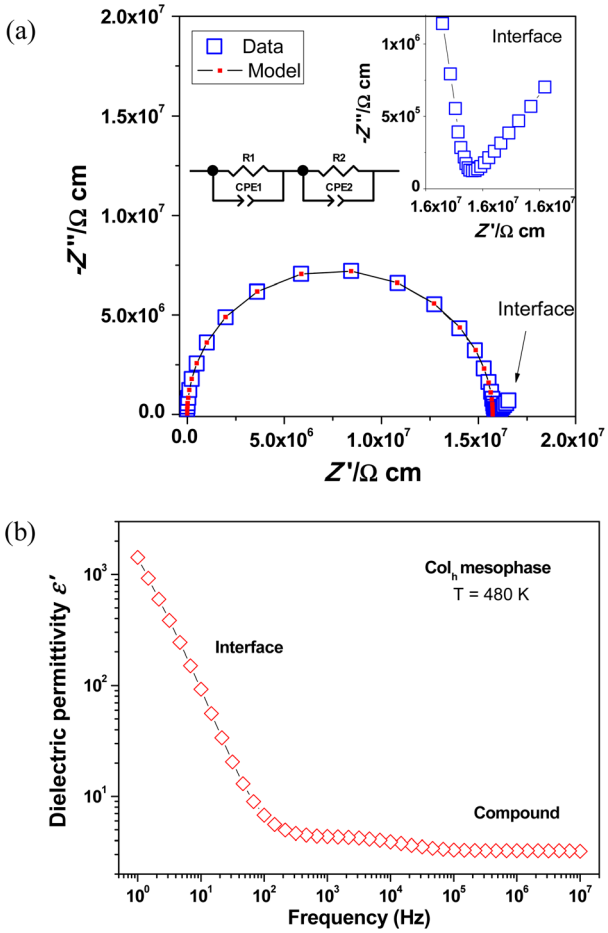

Fig. 4 (a) –*Z*″ *vs.* *Z*′ plot for [Pd(pz$^{R(12,12)iq}$)(pz$^{R(10,10)iq}$)] **4** in the hexagonal columnar mesophase at 560 K (287 °C). The inset displays a magnification of the data recorded in the high-frequency region. The equivalent circuit model used is also shown. (b) Dielectric permittivity curve as a function of frequency recorded for **4** in the Col$_h$ mesophase at 480 K (207 °C).

equivalent circuit fits for both heating and cooling cycles. Fig. 5 displays the σ' *vs.* T plots for the prototype compound **4**. It is interesting to note that proton conduction sets in at low temperatures near to 25 °C, when the nanochannels are opened in the columnar mesophases. Since the σ' values do not drastically change at the Col_r–Col_h phase transition, it is likely that the required continuous pathways for proton conduction are also formed in the Col_r mesophase. However, the slope of the conductivity curves is slightly different in both mesophases, which suggest that proton transfer between molecules may not be equally favoured in the Col_r and Col_h phases. The activation energies E_A were calculated from the Arrhenius plots of $\ln \sigma'$ *vs.* $1/T$ as indicated in Fig. 5 where the E_A values in the Col_r mesophase are higher than for the Col_h one. This feature indicates that the supramolecular organisation in the Col_r mesophase may be less favourable for proton conduction through the nanochannels, although both types of mesophases seem to form the required nanochannels.

The σ' *vs.* $1/T$ curves for all Pd(II) metallomesogens analysed are shown in Fig. 6, in the temperature range of the Col_h mesophases. The E_A values were calculated to be in the range of 0.5–1.15 eV, which are typical values for proton conduction. Based on previous results reported for similar bispyrazolate-based species, the chain length does not seems to be a major factor on the activation energy.[16,24] However, it was found that the type of arrangement in the mesophase clearly affects the proton conduction. In tetragonal columnar (Col_t) and lamellar columnar (Col_L) mesophases, high E_A values ranging between 1.5 eV and 3.0 eV have been reported for analogous compounds,[16,21] whereas in Col_r and Col_h mesophases, the E_A values are usually lowest, ranging between 0.7–1.2 eV.[16,24] This indicates that the proton jump from the donor to the acceptor sites is more favourable in Col_r and Col_h mesophases, in terms of the energy costs. In this context, it is interesting to note that compounds **2** and **4** form a Col_r mesophase before the formation of the Col_h one upon heating, whereas compounds **5** and **7** directly form the

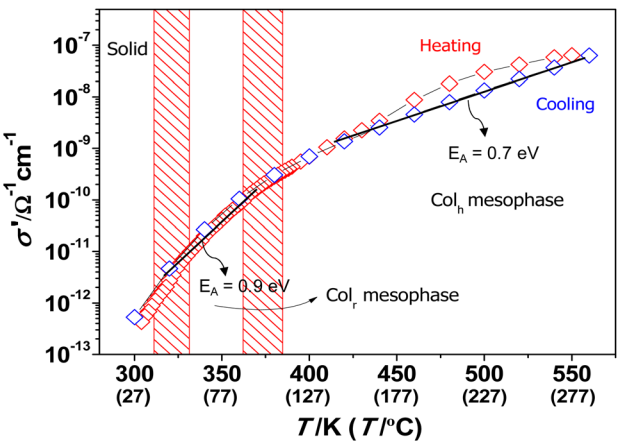

Fig. 5 σ' *vs.* T plots for [Pd($pz^{R(12,12)iq}$)($pz^{R(10,10)iq}$)] **4** at variable temperature (given in Kelvin and °C). The red shaded areas show the solid (Cr)–mesophase (Col_r) and mesophase (Col_r)–mesophase (Col_h) phase transitions established by DSC.

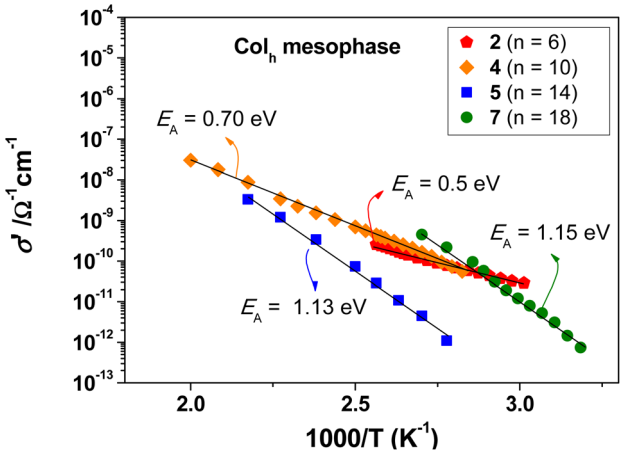

Fig. 6 σ' *vs.* $1000/T$ curves extracted from the equivalent circuit fits for the Pd(II) metallomesogens [Pd($pz^{R(12,12)iq}$)($pz^{R(n,n)iq}$)] **2**, **4**, **5** and **7**, in the hexagonal columnar mesophase. The values of the respective activation energies E_A are indicated.

Col_h mesophase from the solid. Compounds **2** and **4** exhibit lower E_A values in the Col_h mesophase as compared to **5** and **7**, constituting a further improvement with respect to Col_t and Col_L mesophases. It may be concluded that the pre-existing Col_r mesophase favours the formation of a more conducting Col_h mesophase, where the higher conductivity may be associated with improved cooperative motions of the molecules facilitating proton jumps with lower energy costs.

The maximum conductivity σ' values in the order of 10^{-8}–10^{-7} Ω^{-1} cm^{-1} were measured in the Col_h mesophases for compounds **4** and **5**, bearing intermediate chain lengths (Table S1†). Note that the upper instrumental limit for conductivity measurements is 289 °C, whereas the Col_h mesophases are highly stable up to 412 °C. This implies that the conductivity values in the mesophase at higher temperatures above 300 °C or in the isotropic liquid are not accessible, but can be expected to reach considerably higher values.

Similar features were described for analogous symmetrical Pd(II) compounds, which showed proton conductivities ranging between 10^{-10} and 10^{-6} Ω^{-1} cm^{-1} (see Table S1†).[16,24] These values are similar, but the introduction of asymmetry into the compounds allowed extending the stability temperature range of the mesophases and thus extending the low-temperature limit where proton conduction sets in. This increase of the operational temperature range of the metallomesogens investigated is a key factor that renders their Col_h mesophases an efficient platform for the development of new ion conductors.

Conclusions

The introduction of asymmetry and the functionalisation of the pyrazolate ligands with an isoquinoline moiety has been employed as a joint strategy to improve the mesomorphic behaviour of Pd(II) metallomesogens bearing two pyrazolate

ligands. All compounds show columnar mesophases with surprisingly low melting temperatures in the range of 42–61 °C, whereas isotropization occurs at temperatures above 300 °C. This means that the stability ranges of the mesophases exceed 280 °C, being able to reach values of up to 351 °C when the compound is decorated with aliphatic chains of 12 and 8 carbon atoms. Encouraged by these results and keeping in mind the potential application of these materials as water-free electrolytes, their charge transport properties have been analysed. It was found that the nanochannels formed in the columnar mesophases at temperatures near to room temperature may act as continuous pathways for 1D proton conduction. Moreover, proton conduction occurs in the absence of water or humidity, since the fluidic state of the mesophase favours the mobility of the charge carriers. The conductivity values are not excessively promising though, most likely due to the fact that the proton conduction mechanism is based on a C–H···N proton transfer, which may not be energetically favourable.

For future work it is suggested that the unsymmetrical pyrazolate-based Pd(II) metallomesonges presented here may be promising candidates to fabricate various one-dimensional ionic conductors by incorporating ions such as Li^+, Na^+, K^+ or Mg^{2+} into the structure near the nanochannels.

Conflicts of interest

The authors declare no conflicts of interest.

Acknowledgements

This work was supported by the Spanish Ministerio de Economía y Competitividad (project CTQ2015-63858-P (MINECO/FEDER)), Ministerio de Ciencia e Innovación (project PID2020-118078RB-100), and Comunidad Autónoma de Madrid (project Y2020/NMT-6661). C. Cuerva acknowledges the Universidad Complutense de Madrid for his predoctoral contract in 2015–2017 (Programa de Financiación de Universidad Complutense de Madrid-Santander Universidades (CT4/14)).

References

1 S. J. Kim, S. H. Kang, K.-M. Park, H. Kim, W.-C. Zin, M.-G. Choi and K. Kim, *Chem. Mater.*, 1998, **10**, 1889–1893.
2 R. Giménez, O. Crespo, B. Diosdado and A. Elduque, *J. Mater. Chem. C*, 2020, **8**, 6552–6557.
3 L. Soria, M. Cano, J. A. Campo, M. R. Torres and C. Lodeiro, *Polyhedron*, 2017, **125**, 141–150.
4 E. Beltrán, J. Barberá, J. L. Serrano, A. Elduque and R. Giménez, *Eur. J. Inorg. Chem.*, 2014, **2014**, 1165–1173.
5 A. Kishimura, T. Yamashita and T. Aida, *J. Am. Chem. Soc.*, 2005, **127**, 179–183.
6 J. Barberá, A. Elduque, R. Giménez, L. A. Oro and J. L. Serrano, *Angew. Chem., Int. Ed. Engl.*, 1996, **35**, 2832–2835.
7 H. O. Lintang, K. Kinbara, K. Tanaka, T. Yamashita and T. Aida, *Angew. Chem., Int. Ed.*, 2010, **49**, 4241–4245.
8 J. Barberá, I. Lantero, S. Moyano, J. L. Serrano, A. Elduque and R. Giménez, *Chem. – Eur. J.*, 2010, **16**, 14545–14553.
9 A. Sachse, S. Demeshko, S. Dechert, V. Daebel, A. Lange and F. Meyer, *Dalton Trans.*, 2010, **39**, 3903–3914.
10 C.-H. Tseng, M. A. Fox, J.-L. Liao, C.-H. Ku, Z.-T. Sie, C.-H. Chang, J.-Y. Wang, Z.-N. Chen, G.-H. Lee and Y. Chi, *J. Mater. Chem. C*, 2017, **5**, 1420–1435.
11 C. S. Hawes and P. E. Kruger, *Crystals*, 2014, **4**, 32–41.
12 M. C. Torralba, M. Cano, S. Gómez, J. A. Campo, J. V. Heras, J. Perles and C. Ruiz-Valero, *J. Org. Chem.*, 2003, **682**, 26–34.
13 P. Ovejero, E. Asensio, J. V. Heras, J. A. Campo, M. Cano, M. R. Torres, C. Núñez and C. Lodeiro, *Dalton Trans.*, 2013, **42**, 2107–2120.
14 C.-T. Liao, H.-H. Chen, H.-F. Hsu, A. Poloek, H.-H. Yeh, Y. Chi, K.-W. Wang, C.-H. Lai, G.-H. Lee, C.-W. Shih and P.-T. Chou, *Chem. – Eur. J.*, 2011, **17**, 546–556.
15 S.-H. Liu, M.-S. Lin, L.-Y. Chen, Y.-H. Hong, C.-H. Tsai, C.-C. Wu, A. Poloek, Y. Chi, C.-A. Chen, S. H. Chen and H.-F. Hsu, *Org. Electron.*, 2011, **12**, 15–21.
16 C. Cuerva, J. A. Campo, M. Cano and R. Schmidt, *Dalton Trans.*, 2017, **46**, 96–105.
17 I. Sánchez, M. J. Mayoral, P. Ovejero, J. A. Campo, J. V. Heras, M. Cano and C. Lodeiro, *New J. Chem.*, 2010, **34**, 2937–2942.
18 I. Sánchez, C. Núñez, J. A. Campo, M. R. Torres, M. Cano and C. Lodeiro, *J. Mater. Chem. C*, 2014, **2**, 9653–9665.
19 K. D. Katariya, K. J. Nakum, R. Soni, S. S. Soman and M. Hagar, *J. Mol. Liq.*, 2022, **357**, 119073.
20 C. Cuerva, J. A. Campo, M. Cano and C. Lodeiro, *Chem. – Eur. J.*, 2016, **22**, 10168–10178.
21 C. Cuerva, J. A. Campo, M. Cano and R. Schmidt, *J. Mater. Chem. C*, 2019, **7**, 10318–10330.
22 J. Seo, S. Kim, S. H. Gihm, C. R. Park and S. Y. Park, *J. Mater. Chem.*, 2007, **17**, 5052–5057.
23 C. Cuerva, J. A. Campo, P. Ovejero, M. R. Torres and M. Cano, *Dalton Trans.*, 2014, **43**, 8849–8860.
24 C. Cuerva, J. A. Campo, M. Cano, J. Sanz, I. Sobrados, V. Diez-Gómez, A. Rivera-Calzada and R. Schmidt, *Inorg. Chem.*, 2016, **55**, 6995–7002.
25 C. Yin, J. Li, Y. Zhou, H. Zhang, P. Fang and C. He, *ACS Appl. Mater. Interfaces*, 2018, **10**, 14026–14035.